



Investigations of rare earth and radioactive elements in black sands of Kerala Beach using spectroscopic techniques

V. K. Shukla¹ · Abhishek Kr. Rai² · A. Dwivedi¹ ·
A. K. Rai¹

Received: 9 August 2023 / Accepted: 5 October 2023 / Published online: 3 November 2023
© The Author(s), under exclusive licence to The Optical Society of India 2023

Abstract The present manuscript deals with the identification of the spectral lines of the rare earth elements (REEs) in the LIBS spectra of the black sands collected from the Thiruvananthapuram (Kerala) beach using laser-induced breakdown spectroscopy (LIBS). LIBS spectra of the sand sample show the presence of spectral lines of Na, Mg, Mn, Al, and Cr. Along with these elements, the spectral lines of REEs such as Ce, Nd, Sm, Dy, Ho, Tm, etc., and the radioactive element Thorium (Th) are also present in the LIBS spectra of the black sand sample. The presence of REEs and radioactive elements makes the sand suitable for profitable extraction using various methods for different applications. The results of LIBS (presence of all REEs in sand) are also verified by photoacoustic spectroscopy (PAS). The Plasma temperature has been calculated using the Boltzmann plot to explain the distribution of the atoms in various higher energy states/levels. An attempt is made to explain the various transitions involved in the spectral lines of the rare earth ions in the LIBS spectra of the black sand sample using a possible energy level diagram. The concentration of some REEs (Dy, Sm, and Nd) and LOD has been calculated by using the calibration curve method. To the best of our knowledge, the investigation of rare earth and radioactive elements in the black sand of the Kerala beach using LIBS is reported for the first time.

Keywords LIBS · Photoacoustic spectroscopy · Rare earth elements · Plasma temperature · Calibration curve · Limit of detection

Introduction

Rare earth elements (REEs) are grouped into two types i.e., the lanthanide series, which contains the elements La, Ce, Pr, Nd, Pm, Sm, Eu, Gd, Tb, Dy, Ho, Er, Tm, Yb, Lu and the actinide series as Ac, Th, Pa, U, Np, Pu, etc. REEs show unique properties such as optical, magnetic, and catalytic, due to which REEs are used in several modern technologies (i.e., computers, cellular phones, permanent magnets, motors for wind turbines and disk drives, hybrid car batteries, compact fluorescent lighting, automobile catalytic converters, etc.) [1–3].

Traditionally, REEs are extracted from natural mineral deposits. It has been reported that many rare earth elements are found in the Earth's crust as minerals [4–6]. Due to the sedimentary process (erosion, weathering, etc.), the REEs and other elements (Ti, Zr, Fe, etc.) are usually present in coastal areas. It has been carried out by rivers, which usually pass through rocks, minerals along the beaches, etc. [7]. Beach Sands show some significant variation in their compositions of REEs (Ce, Dy, etc.) depending upon the origin of rocks from which they are formed [7].

Radioactive elements (Thorium and Uranium) are commonly associated with REE-bearing minerals where the concentration depends on the mineral, the formation of the rocks, and the geographical position of the deposit [8]. The natural radioactivity due to the presence of U (238), and Th (232), and the artificial radioactivity due to ¹³⁷Cs in beach sand samples from the Black Sea coast of Kocaeli (Turkey) have been measured by gamma-ray spectroscopy [9].

✉ A. K. Rai
awadheshkrai@rediffmail.com

¹ Laser Spectroscopy Research Laboratory, Department of Physics, University of Allahabad, Prayagraj 211002, India

² Department of Earth and Planetary Science, University of Allahabad, Prayagraj 211002, India

India has a long coastal line. The coastline of the continent, Lakshadweep Islands and Andaman & Nicobar Islands is 7516.6 km. Many elements have been reported in the Indian beach sand. REEs such as Ce, La, Nd, Pr, Sm, Gd, and Dy have been found along India's seashore of the east area of Andhra Pradesh [10]. Radiogenic and heavy minerals such as Th, U, and K have been found significantly on the beach at India's Chhatarpur coast of Orissa state [11]. The Thorium deposits on the West Coast (Kerala) are believed to be washed down from highlands and have been deposited through rivers or water streams [11].

Black sands usually occur black and consist of a heavy, smooth, glossy, and partly magnetic mixture of fine sands. The black sands are an important economic deposit of resistant and high specific gravity minerals formed by the process of mechanical concentration due to sedimentary process (erosion transportation and deposition) at suitable locations. The black sand sample has been collected from various places and analyzed by various analytical techniques such as Gamma-ray spectroscopy in which Th, Ra, and K have been reported [12], and the ICPMS technique in which garnet, monazite, etc. have been reported [13], the electromagnetic and electrostatic technique in which concentration of monazite (REEs) of Egyptian beach black sand has been determined [14], and various numerical modelling technique has been used to quantify the concentration of elements present in the black sand sample [15, 16]. All these mentioned techniques require tedious sample preparation and not multi-elemental analytical techniques. Therefore, in the present work, we have tried to analyze the rare earth elements with the LIBS and PAS techniques. LIBS is a versatile technique for quantitative analysis of various contaminants, including radioactive elements in a wide range of samples, including sand soils, sediments, and other geological materials [17–20]. LIBS is also helpful for the in-situ, i.e., without sample preparation and multi-elemental analysis, and can be used for trace element identification in minerals/geological samples.

In the present work, the elemental analysis of black sands obtained from Thiruvananthapuram (Kerala) has been performed using the LIBS technique. The mechanism of various transitions in rare-earth ions is well explained using an energy level diagram. The presence of rare earth elements is further confirmed via the PAS technique. In this work, our main objective is to detect and quantify REEs such as Tm, Ho, Dy, Ce, Sm, and Nd and a radioactive element such as Thorium (Th) in black sands using LIBS.

Experimental details

The sand sample had been collected from the Indian Beach named Thiruvananthapuram (Kerala). The sample was

washed three times with distilled water. The sample was poured on a Petri dish and held in an oven (MAC-MSW-211) for 4–5 h at 105 °C to desiccate the sample. The dried sample was powdered by using the agate mortar and pestle. The powdered sand was sieved with a 120 µm sieving machine. Finally, a small pellet (having a diameter of 1 cm) of the sieved sand sample was made using a Press Machine (K-Br Press MODEL M-15) with a pressure of 1200 bar.

LIBS experimental set-up

The LIBS spectra of these pellets were recorded using the LIBS experimental setup with suitable acquisition parameters optimized at 1 µs gate delay, 1.5 µs gate width, and pulse energy 15 mJ/pulse. A schematic of the experimental set-up shown in Fig. 1 is used to record the LIBS spectra of the samples studied in the present work. The experimental setup comprises a Q-switched Nd-YAG laser (Continuum, Surelite III-10 USA), a lens having a focal length of 15 cm, movable sample stage (to avoid crater formation), collection optics (UV-NIR light collection ME OPT007, Andor Technology, USA), spectrograph, integrated charge-coupled device (ICCD) (iStar334, Andor Technology, USA), energy meter (Genetec-e model UP19K-30H-VM-DO) and digital delay generator (Stanford Research System-DG535) [21].

The Nd: YAG laser, having a maximum pulse energy of 425 mJ, pulse duration (FWHM) 4 ns, and a repetition rate of (1–10) Hz, is focused at the surface of the sand sample, which finally results in the plasma formation. Light emitted from the plasma is collected using collecting optics and finally fed to the entrance slit of the spectrograph with the help of optical fiber. The spectrograph is equipped with an ICCD camera. The camera is connected to a computer, and the LIBS spectrum can be seen on the computer desktop screen. The excellent signal-to-noise ratio(S/N) and signal-to-background ratio(S/B) are obtained at 1 µs gate delay, 1.5 µs gate width, and at 15 mJ/pulse energy.

PAS experimental setup

The PAS spectrum of powdered sand samples was recorded using a broadband source, a Xenon Arc Lamp (HORIBA Canada, OBB Corporation). A 30 Hz chopper modulation frequency obtained from a mechanical chopper (model SR-540, Stanford, USA) was chosen. The PA signal from the condenser microphone was detected with a lock-in amplifier (model SR-830), with a time constant of 10 s, and recorded by a PC as a function of the wavelength from the monochromator (MD-2000 USB motor controller). Further discussion of the PAS experimental setup has been addressed by Gazali et al. [22].

Fig. 1 Schematic diagram of the experimental set-up of the LIBS

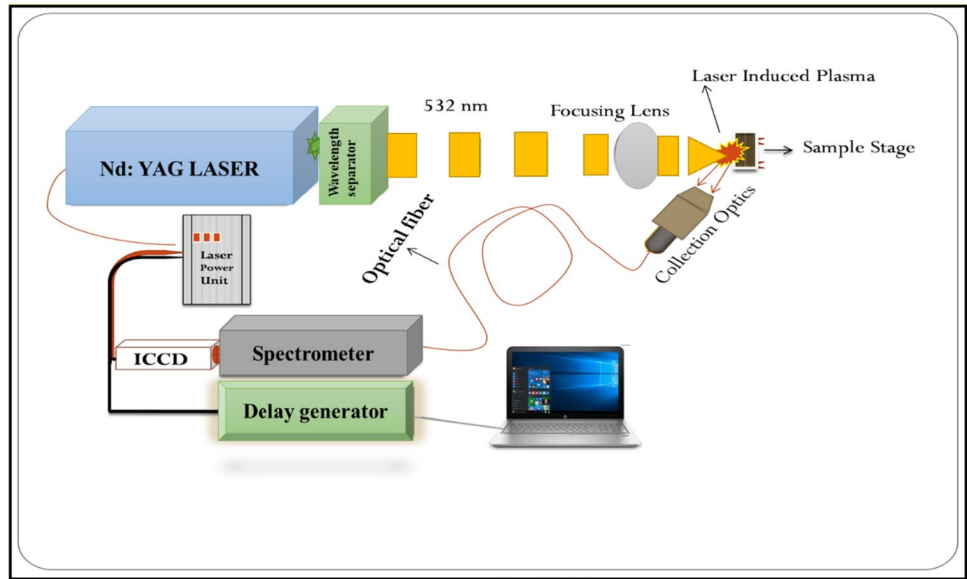
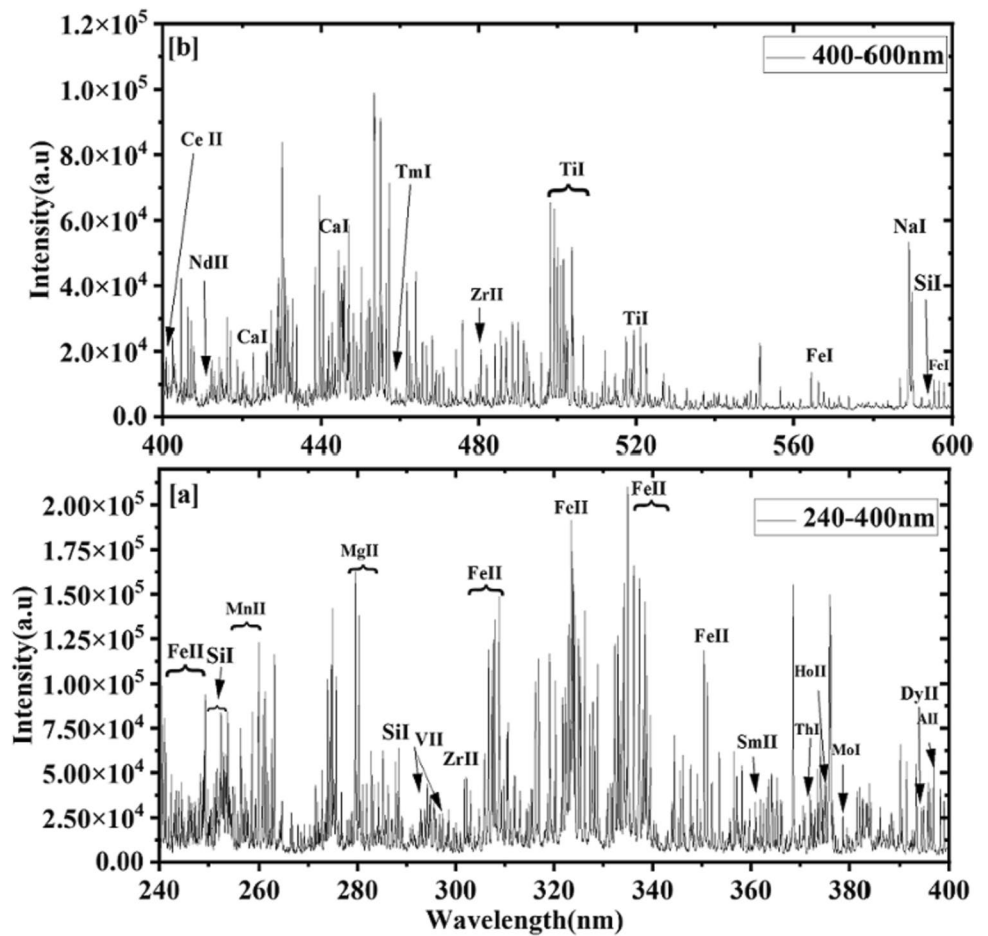


Fig. 2 a, b LIBS spectra Black sand sample (240–600) nm



Results and discussion

LIBS spectra

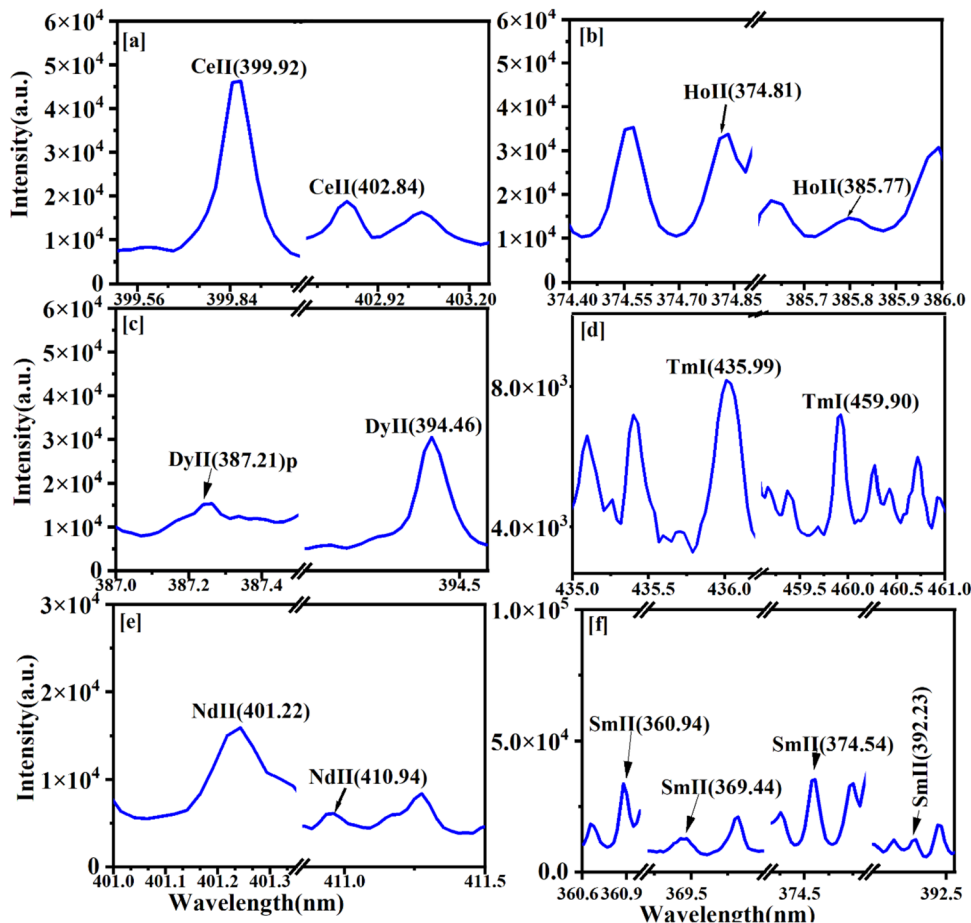
Figures 2a, b show the LIBS spectra of the black sand in the range of 240–600 nm. Spectral signatures of some common elements like Fe, Ti, Mn, spectral lines of REEs, and radioactive elements are observed in the LIBS spectra

of the sand samples in Fig. 2a, b. Multiple peaks of Fe and Ti are observed in the LIBS spectra of the sand sample. The intensities, as well as the numbers of spectral lines of Fe and Ti, are very large in the LIBS spectra, which confirms the presence of a large amount of Fe and Ti. In this work, our main concern is towards the RE elements such as Tm, Ho, Dy, Ce, Sm, and Nd and a radioactive element such as Thorium (Th), which have been detected in the LIBS spectra of the black sand samples.

Table 1 wavelength corresponds to the spectral lines of the radioactive and REEs

Sr. No.	Elements	Wavelength (nm)
1	Th	371.9(I),400.8(I),412.7(I)
2	Ce	383.8(II),393.9(II)p,402.8(II),407.1(II)
3	Dy	338.5(II),340.7(II),353.1(II),387.2(II)p,394.4(II),396.8(II),400.0(II), 404.5(I), 416.7(I), 418.6(I), 419.4(I),421.1(I)
4	Sm	360.9(II),369.3(II),374.5(II)p,392.2(II), 425.6(II), 428.0(II), 429.6(I), 434.6(I), 447.0(II)p, 475.9(I), 484.1(I), 507.1(II)
5	Nd	379.6(II), 385.3(II). 386.5(II)401.2(II)p,410.9(II)p,424.7(II)p,463.3(II)
6	Tm	313.1(II), 346.2(II),44(I)0, 362.2(I),371.7(I),384.8(II), 418.7(I), 435.9(I)p,459.9(I)
7	Ho	379.7(II),380.2(II),404.6(I)

Fig. 3 LIBS spectra of the RE elements, i.e. **a** Ce, **b** Ho, **c** Dy, **d** Tm, **e** Nd, and **f** Sm



Analysis of the spectral lines of REEs in LIBS spectra of black sand

Several spectral lines of the REEs are present in the LIBS spectra of black sand samples. The spectral lines of REEs may be seen in Fig. 2 and have been summarized in Table 1. Some spectral lines of these REEs are overlapped with the spectral lines of Fe, Zr, Mn, and Ti. Figure 3a–f shows the sharp and distinct spectral lines of Ce, Ho, Dy, Tm, Nd, and Sm, respectively. In the case of Ce II, two well-separated lines are observed at 399.9 and 402.8 nm (Fig. 3a). Similarly, the spectral lines of Ho II are observed at (374.8, 385.7 nm), Dy II at (387.2, 394.4 nm), Tm I at (435.9, 459.9 nm), Nd II at (401.2, 410.9 nm) and Sm II at (360.9, 369.4, 374.5, 392.2 nm) as shown in Fig. 3b–f, respectively.

Since, there is an overlapping of spectral lines of rare earth elements with the spectral lines of Zr, Fe, Ti, and Mn elements, the deconvolution is performed in the overlapped region of rare earth elements with Fe/Zr/Mn/Ti elements. Figure 4a–f shows the deconvoluted spectra of Ce II, Ho II, Dy II, Tm II, Nd II, and Sm I elements with the spectral lines of Zr, Fe, Ti, and Mn. The spectra show that some of the persistent lines of rare earth elements are merged with spectral lines of other elements. So, from deconvoluted spectra, it has been confirmed that all the persistent spectral lines of rare earth elements are present in the LIBS spectra of the

sand sample. Figures 4a–f show the spectral overlapping of Ce with Zr, Ho with Fe, Dy with Fe; Tm with Fe/Ti; Nd with Mn/V/Fe, and Sm with Ti, respectively.

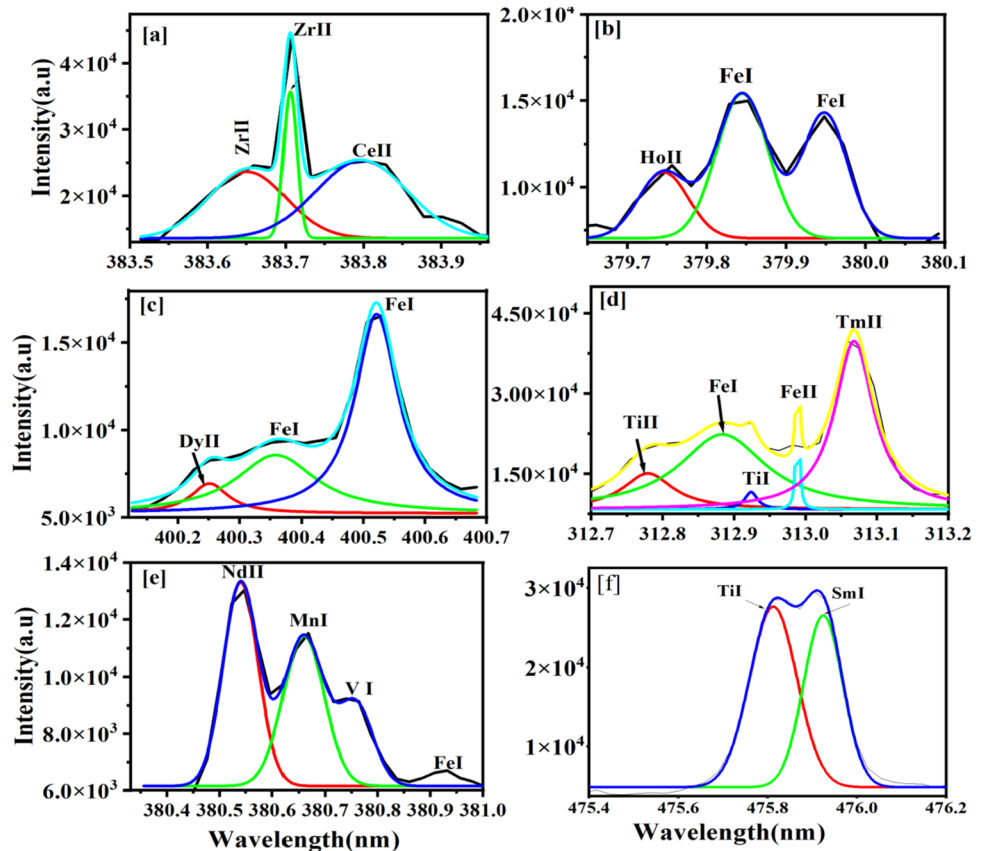
Plasma temperature

The light emitted from laser-induced plasma (LIP) of the sample surface is an important asset for the qualitative and quantitative analysis of the test sample and for studying the plasma properties. The fundamental properties of plasma are plasma temperature, electron density, and the number density of the emitting species [29].

The intensity of the spectral lines of the elements represents its concentration in the sample. But for the quantitative analysis of the constituents based on the intensity of the spectral lines of the elements, the laser-induced plasma should satisfy the following three conditions (i) it should be stoichiometric, (ii) it should be optically thin (iii) it should be in local thermodynamic equilibrium (LTE).

- (i) For the true representation of the sample by the Laser-induced plasma, plasma must satisfy the stoichiometric condition. The Laser-induced plasma is said to be stoichiometric if the Laser irradiance is more than the threshold value, i.e., 10^9 W cm^{-2} . The power density corresponding to 15 J mJ laser energy, 4 ns pulse

Fig. 4 Deconvoluted spectra of different REEs, i.e. **a** Ce (383.8 nm), **b** Ho (379.7 nm), **c** Dy (400.0 nm), **d** Tm (459.9 nm), **e** Nd (379.6 nm) and **f** Sm (475.9 nm)



duration, and 36 μm focal spot is 3.0 × 10¹² W cm⁻², which satisfies the condition of stoichiometric laser ablation from the sample [17].

- (ii) There could be the possibility that the Photons emitted by the excited atom in the inner core of the plasma can be absorbed by the atoms in the ground state, which results in a self-absorption line present in the LIBS spectra. The spectral intensity ratio of two spectral lines having nearly similar upper energy levels is compared with the ratio of their A_{ki}, g_k, and λ⁻¹ to ensure the optical thinness of the plasma. For the optically thin plasma, two spectral lines, the intensity ratio (I/I') should be nearly the same as (A_{ki} g_k λ' / A'_{ki} g_k λ) [23]. In our experiment, we verified the spectral lines of the Aluminium element in our sample. The ratio of I/I' = 0.5623 ± 6% (according to the ratio of the intensity of the two lines of aluminum at wavelength 394.6 nm and 396.1 nm found in the LIBS spectra) and the theoretical calculation for the lines of Aluminium at above-mentioned wavelength of the sample is (A_{ki} g_k λ' / A'_{ki} g_k λ) = 0.5445 ± 4%. Hence, we see that both values are nearly the same. Thus, we can conclude that plasma is optically thin.
- (iii) The condition of local thermal equilibrium (LTE) requires

$$N_e \geq 1.6 \times 10^{12} T^{1/2} [\Delta E]^3 \tag{1}$$

where N_e (cm⁻³) is the electron density, T (K) is the plasma temperature, and E (ev) is the largest energy transition. To satisfy the above condition, we have calculated the Plasma temperature for the elements Aluminium and iron elements having wavelength listed in Table 2.

The calculation has been done using the following formula [24]:

The emission line intensity (I_{ji}) corresponding to the transition between the upper level (j) and the lower level (i) can be expressed as follows.

$$I_{ji} = F \cdot C_s \cdot A_{ji} g_j \cdot \exp\left(-\frac{E_j}{K_B T}\right) / U_s(T) \tag{2}$$

here, F is the experimental parameter that accounts for the optical efficiency of the collection system, C_s is the emitting species concentration, A_{ji} is the transition probability, g_j gives jth level degeneracy, E_j energy at jth level, K_B represents the Boltzmann constant, U_s(T) is the partition function, and T is the plasma temperature.

The partition function at a particular plasma temperature can be calculated as follows;

$$U_s(T) = \sum_{j=1}^n g_j \exp\left(-\frac{E_j}{K_B T}\right) \tag{3}$$

As required in Eq. (2) and Eq. (3), the plasma temperature was extracted using the Boltzmann plot method, a graphical representation of a group of spectral lines of emitting species.

Taking logarithm on both sides of Eq. (2) and arranging it in the form of a linear equation:

$$\ln\left[\frac{I_{ji}}{A_{ji} g_j}\right] = \frac{-E_j}{K_B T} + \ln[F \cdot C_s / U_s(T)] \tag{4}$$

Compared with the standard linear equation, it gives slope (m) and intercepts (q_s) as follows;

$$Y_k = \ln(I_{ji} / (A_{ji} g_j)), X_k = E_j, m = -\frac{1}{K_B T}, q_s = \ln[F \cdot C_s / U_s(T)] \tag{5}$$

In Boltzmann's plot, the term (E_j, ln [I_{ji}/A_{ji} g_j]) can be represented as a point (X_K, Y_K), and these points are fitted with a straight line which gives slope and intercepts as shown in Fig. 5. The slope is used to find the plasma temperature.

By putting the value of E_j and Temperature (T), we have calculated the value of N_e (1.5 × 10²⁰ ± 5%)/cm³.

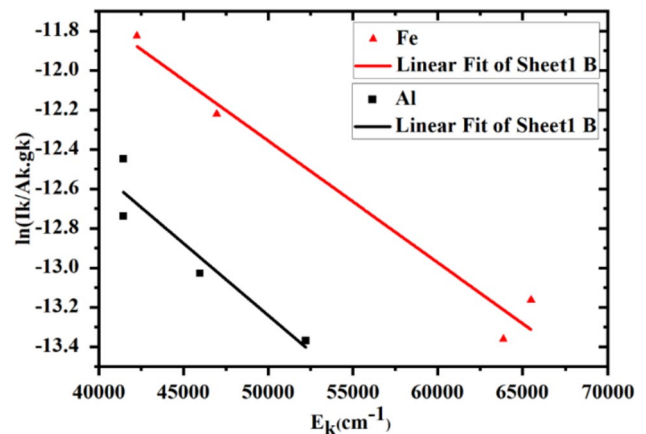


Fig. 5 Boltzmann Plot of the Fe and Al elements in LIBS spectra of the Black-Sand

Table 2 Plasma temperature calculated for the different lines of Fe and Al

Sr. No.	Elements	Wavelengths (nm)	Plasma temperature	R ² (COD)
1	Fe	233.2(II),242.4(II),251.1(II),253.6(II)	19,500 ± 400	0.9694
2	Al	237.3(I),308.2(I), 394.4(I),396.1(I)	20,100 ± 300	0.8902

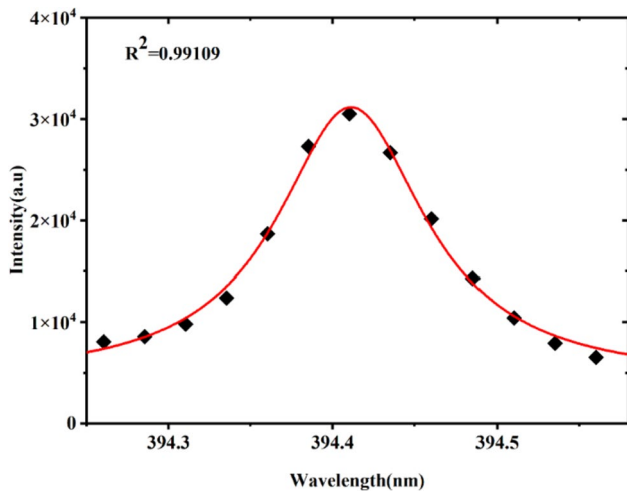


Fig. 6 Lorentzian fit of the Al (I) spectral profile at wavelength 394.4 nm

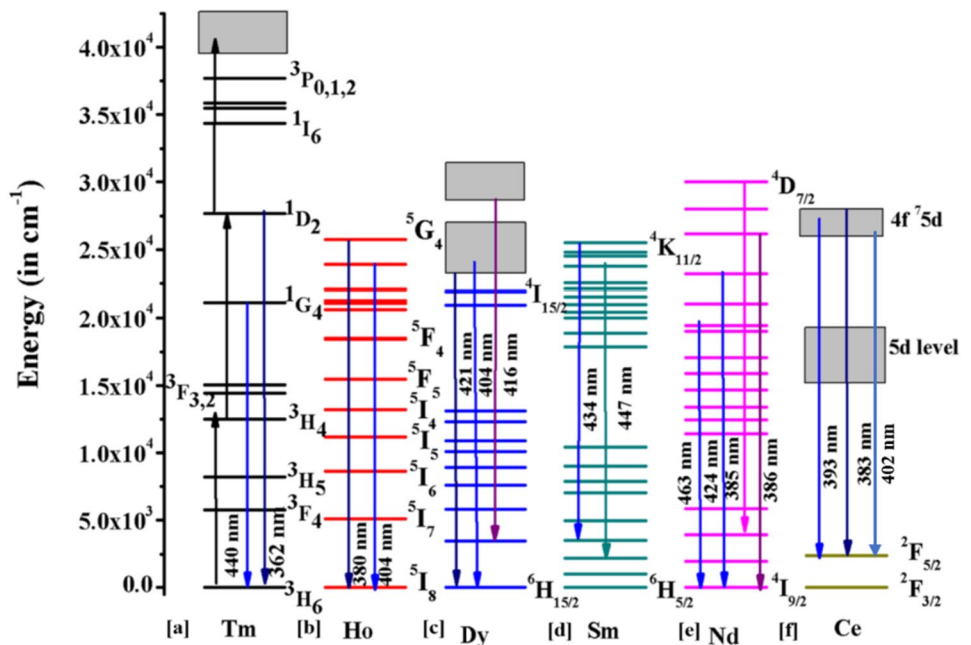
The electron density may be calculated by measuring the full width at half maxima of the stark broadened line given by the expression:

$$N_e = (10^{16} \Delta\lambda) / 2w \tag{6}$$

Here, w is the electron parameter whose value is 9.36×10^{-4} nm for the aluminum line at the wavelength (394.4 nm), and $\Delta\lambda$ has been calculated by using the formula

$$\Delta\lambda = \left(\Delta\lambda_{\text{observed}}^2 - \Delta\lambda_{\text{spectrometer}}^2 \right) \tag{7}$$

Fig. 7 Possible energy level diagram of Tm, Ho, Dy, Sm, Nd, and Ce ions



Where the full width at half maximum ($\Delta\lambda_{1/2}$) of these lines has been extracted by fitting the Lorentzian function over the line profile as shown in Fig. 6. The lower limit value of electron density N_e , by satisfying Mcwhirter criteria using Eq. (1), is $1.5 \times 10^{20} \pm 5\% / \text{cm}^3$, and N_e has been calculated using Eq. (6) is $5.9 \times 10^{22} \pm 8\% / \text{cm}^3$. It is clear from the calculation that the electron number density is greater than the electron density of a lower limit. Thus, the condition of LTE is satisfied.

Mechanism of excitation of REEs at various levels

The mechanism behind the different transitions of rare earth elements in black sands is explained with the help of plasma temperature and the possible energy level diagram. The plasma temperature is calculated via a Boltzmann plot, which is around $19,500 \pm 400$ K. The energy corresponding to the plasma temperature is $13,554 \text{ cm}^{-1}$ (i.e., 1.6803 eV), and the wavelength associated with this energy is 740 nm. This plasma temperature plays a vital role in the excitation of the different levels of REEs present in the black sand. Figure 7a–f shows the energy level diagram of Tm, Ho, Dy, Ce, Nd, and Sm elements. Rare-earth ions have several metastable states [25–27], so the excitation in these levels is due to thermal energy similar to the multiphoton process. In the beginning, the plasma temperature is very high, which is responsible for the population built up in higher levels of rare-earth ions [28, 29]. Some of the metastable states of rare-earth ions are populated after the relaxation from higher levels. Another channel is that the ion in the ground state is promoted to its first excited state via thermal excitation

(i.e., the plasma temperature), and then the ion present in the excited state (i.e., metastable state) is further promoted to the next excited state due to the thermal energy of plasma (i.e., plasma temperature). This process is involved in each rare earth element. Figure 7a shows the energy level diagram of the ‘Tm’ ion in which the ion in the ground state (3H_6) is promoted to an excited level (3H_4) on thermal excitation. Since the 3H_4 level is a metastable state [30], there is again the possibility of further excitation from the 3H_4 level to 1D_2 due to thermal energy (Plasma temperature). The whole mechanism behind the excitation process may be summarized below:

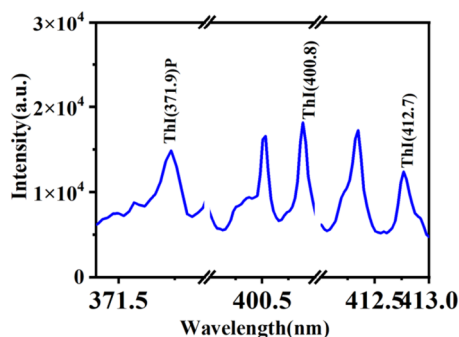
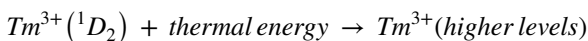
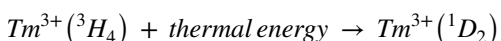
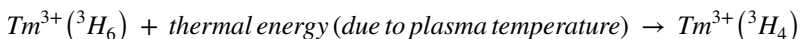


Fig. 8 LIBS spectrum of the black sand sample showing spectral signature of Th I

Fig. 9 Photoacoustic spectrum (PAS) of the black sand sample

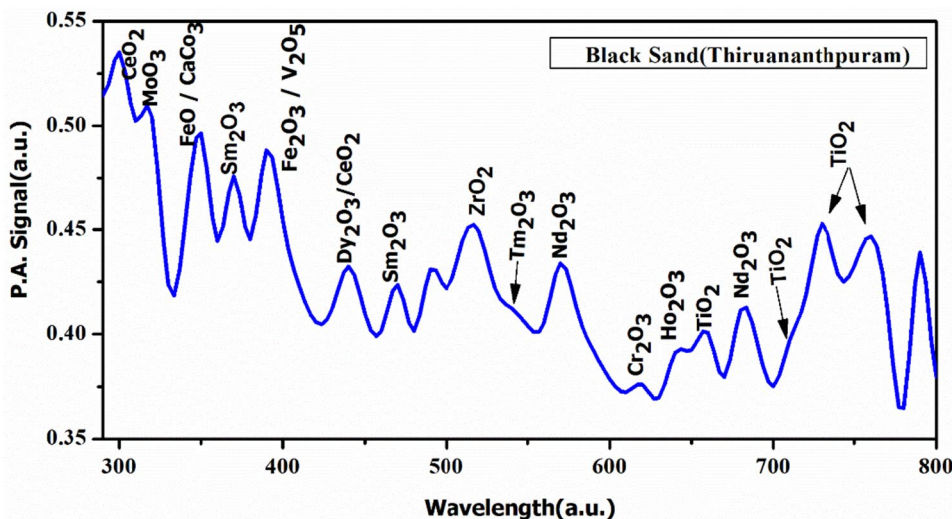


Figure 7b shows the energy level diagram of the Ho ion in which the excitation process is the same as explained in the case of the Tm ion. Similarly, Fig. 7c–f shows the energy level diagram of Dy, Sm, Nd, and Ce ions, respectively, the excitation processes in all REEs may be as explained as in Tm ion. Some of the transitions in different energy levels of these ions are also shown in Fig. 7.

Analysis of the spectral lines of radioactive elements

The beach sand on the West Coast of India, particularly in Kerala, contains one of the richest deposits of thorium in

the world. Several studies on the various aspects of these deposits have been carried out for more than 50 years [11]. Figure 8 shows the LIBS spectrum of black sand in which three persistent lines of Th I at 371.9, 400.8, and 412.7 nm are observed.

Thus, the LIBS spectra show the presence of the spectral lines of REEs, including the radioactive element Th. PAS technique is also used to validate the results of the LIBS technique, i.e., to confirm the presence of REEs in black sand.

Photoacoustic spectrum

Figure 9 shows the PAS spectrum of black sand that shows the absorption bands of various compounds like CeO₂ (300.2 nm), Sm₂O₃ (470.2 nm), Dy₂O₃ (440.5 nm), Tm₂O₃ (540.4 nm), Ho₂O₃ (642.2 nm) and Nd₂O₃ (684.6 nm), ZrO₂ (514.5 nm), TiO₂ (730.4 and 762.5 nm), Cr₂O₃ (617.3 nm)

Table 3 The absorption bands with their peak positions in the PAS spectrum

Sr. No.	Molecular band	PAS peaks found in the Black sand sample (nm)	Absorption spectra in literature (nm)	References
1	CeO ₂	300,2,440	297.0	[31]
2	Sm ₂ O ₃	380	477,408	[32]
4	Ho ₂ O ₃	638	420,640	[32]
5	Nd ₂ O ₃	573	580,750	[32]
6	Dy ₂ O ₃	440	431,455	[32]
7	ZrO ₂	520	530.0	[33]
9	V ₂ O ₅	392	420	[34]
10	CaCo ₃	348	356.2	[35]
11	TiO ₂	660,758	670,0,752	[36, 37]
12	Fe ₂ O ₃ /FeO	349,390	262,0,369,430,487	[38]
13	MoO ₃	317	353.0, 311.0	[39]
14	SiO ₂	543	550	[36]

Table 4 The concentration and LOD of the Dy Sm and Nd

Sr. No.	Elements	Wavelength (nm)	Concentration (ppm)	LOD (ppm)
1	Dy	387.2	226 ± 24.23	128 ± 23.56
2	Sm	360.9	155 ± 16.42	132 ± 18.65
3	Nd	401.2	167 ± 10.28	93.45 ± 19.58

and V₂O₅ (392.5 nm) compounds. The wavelength of the absorption bands of the various compounds available in the literature and the wavelength of the bands of the compounds observed in the PA spectra are compared in Table 3, which shows close agreement.

The presence of these compounds in black sands confirms the presence of rare earth elements in the black sand at Thiruvananthapuram beach, as observed in LIBS spectra.

Calibration curves for the quantitative analysis of REEs

The concentration of some REEs (i.e., Dy, Sm, and Nd) has been determined using the standard calibration curve method. To draw the calibration curves, the standard samples having known amounts (i.e., 1000, 3000, 5000, and 10,000 ppm) of Dy, Sm, and Nd are prepared, and the LIBS spectra of each standard sample are recorded at the same optimized experimental conditions. We choose specific spectral lines of the elements (Table 4), free from interference or having a minimal effect, to draw the calibration curve for determining their concentrations.

We choose the normalized LIBS intensities (Signal to background ratio) of Dy (387.2 nm), Sm (360.9 nm), and Nd (401.2 nm) to draw the calibration curves for Dy, Sm, and Nd, which are shown in Fig. 10a–c. The calibration curve for

each element under investigation is established by plotting the normalized intensity of the specific spectral line of each element as a function of their concentration in ppm. The calibration curve (Fig. 10a–c) shows a linear dependence of the intensities on the concentrations of Dy, Nd, and Sm in the standard sample. The concentrations of Sm, Nd, and Dy are evaluated for the different samples using the above calibration curve and tabulated in Table 4.

Limits of detection

Determining the detection limit of the REEs in the target materials is essential for their extraction from the samples for industrial applications. The basic meaning of the limit of detection is to calculate the lowest concentration that can be detected with the LIBS technique under the optimized condition. The detection limit (LOD) can be estimated by using the equation [40].

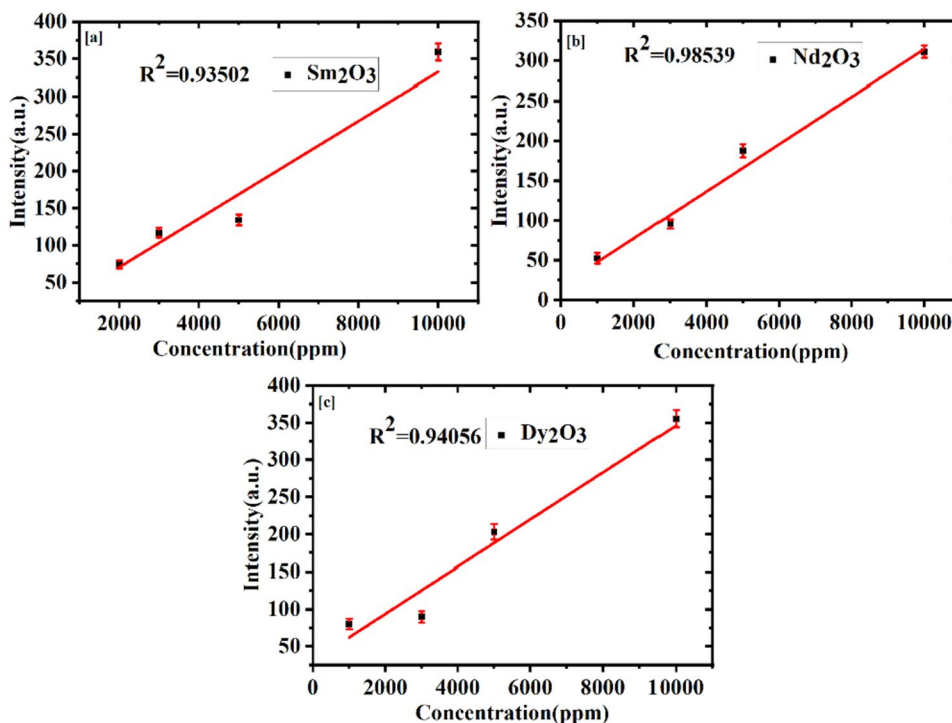
$$LOD = \frac{3\sigma_B}{S} \tag{8}$$

where σ_B is the standard deviation of the background, and S is the slope of the calibration curve. It is clear from the expression that if the slope of the calibration curve (S) is large and the standard deviation of the background is small, then the detection limit is low. The detection limit for the Dy, Sm, and Nd present in the black sand sample is calculated using the above equation and tabulated in Table 4.

Conclusions

The REEs such as Tm, Ho, Dy, Ce, Nd, and Sm are detected in the black sand of Thiruvananthapuram beach using the LIBS technique, which has been reported for

Fig. 10 Calibration curves for a Sm b Nd c Dy



the first time to the best of our knowledge. There is a strong overlapping of the spectral lines of REEs with the spectral lines of common elements like Fe, Ti, etc. Thus, the presence of the spectral lines of REEs is confirmed by deconvolution of the overlapped spectral lines. The mechanism behind the presence of spectral lines of different rare earth elements is explained by comparing the plasma temperature with the energy levels of the rare-earth ions. The excitation process has been explained in this case as similar to the multiphoton process. The radioactive element (i.e., Th) is also observed in LIBS spectra along with rare earth elements. The various compounds containing REEs identified using the PAS technique support the existence of rare earth elements in the black sand samples. Thus, the present manuscript reports a simple, quick, cost-effective, in-situ investigation of REEs and radioactive elements in the black sand samples. The concentration of the Nd ~ 167 ppm, Sm ~ 155 ppm, and Dy ~ 226 ppm is reported in the present manuscript. The estimated values of the LOD for Nd, Sm, and Dy are 93, 132, and 128 ppm, respectively.

Acknowledgements Two authors, Mr. Vineet Kumar Shukla (V.K. Shukla) and Dr. Abhishek Dwivedi, thank UGC, New Delhi, for CRET and Dr. D. S. Kothari for the fellowship as financial support.

Declarations

Conflicts of interest The authors declare no conflict of interest.

References

1. C. Preinfalk, G. Morteani, The industrial applications of rare earth elements. in *Lanthanides, Tantalum and Niobium*. (Springer, Heidelberg, 1989), pp. 359–370
2. W. Weng, A. Biesiekierski, Y. Li, M. Dargusch, C. Wen, A review of the physiological impact of rare earth elements and their uses in biomedical Mg alloys. *Acta Biomater.* **130**, 80–97 (2021)
3. X. Du, T.E. Graedel, Uncovering the end uses of the rare earth elements. *Sci. Total Environ.* **461**, 781–784 (2013)
4. J. Voncken, Mineral processing and extractive metallurgy of the rare earths. in *The Rare Earth Elements* (Springer, Heidelberg, 2016), pp. 73–88
5. N. Rethfeldt, P. Brinkmann, D. Riebe, T. Beitz, N. Köllner, U. Altenberger, H.-G. Löhmannsröben, Detection of rare earth elements in minerals and soils by laser-induced breakdown spectroscopy (LIBS) Using Interval PLS. *Minerals* **11**, 1379 (2021)
6. S. Müller, J.A. Meima, D. Rammlmair, Detecting REE-rich areas in heterogeneous drill cores from Storkwitz using LIBS and a combination of k-means clustering and spatial raster analysis. *J. Geochem. Explor.* **221**, 106697 (2021)
7. K.M. Abedin, A.F.M.Y. Haider, M.A. Rony, Z.H. Khan, Identification of multiple rare earths and associated elements in raw monazite sands by laser-induced breakdown spectroscopy. *Opt. Laser Technol.* **43**, 45–49 (2011)
8. A.C. García, M. Latifi, A. Amini, J. Chaouki, Separation of radioactive elements from rare earth element-bearing minerals. *Metals* **10**, 1524 (2020)
9. S.F. Özmen, A. Cesur, I. Boztosun, M. Yavuz, Distribution of natural and anthropogenic radionuclides in beach sand samples from Mediterranean Coast of Turkey. *Radiat. Phys. Chem.* **103**, 37–44 (2014)
10. J. Palaparathi, R. Chakrabarti, S. Banerjee, R. Guin, S. Ghosal, S. Agrahari, D. Sengupta, Economically viable rare earth element

- deposits along beach placers of Andhra Pradesh, the eastern coast of India. *Arab. J. Geosci.* **10**, 201 (2017)
11. A.K. Mohanty, S.K. Das, K.V. Van, D. Sengupta, S.K. Saha, Radiogenic heavy minerals in Chhatrapur beach placer deposit of Orissa, southeastern coast of India. *J. Radioanal. Nucl. Chem.* **258**, 383–389 (2003)
 12. M. Iyer, Origin of thorium deposits in Kerala beach sands. *Radi. Prote. Envir.* **38**, 98 (2015)
 13. H. Mahmoud, A. Abdel-Lateef, A. Attiah, Distribution of some elements in the Egyptian black sands from Abu Khashaba beach area. *J. Anal. Methods Chem. Instru.* **5**, 62–66 (2013)
 14. M.I. Moustafa, N.A. Abdelfattah, Physical and chemical beneficiation of the Egyptian beach monazite. *Resour. Geol.* **60**, 288–299 (2010)
 15. K. Black, N. Kurian, J. Mathew, M. Baba, Open coast monsoonal beach dynamics. *J. Coast. Res.* **24**, 1–12 (2008)
 16. M. Martin, R.C. Martin, S. Allman, D. Brice, A. Wymore, N. Andre, Quantification of rare earth elements using laser-induced breakdown spectroscopy. *Spectrochim. Acta Part B At. Spectrosc.* **114**, 65–73 (2015)
 17. G. Ravindra Kumar, and C. Sreejith, Relationship between heavy mineral placer deposits and hinterland rocks of southern Kerala: a new approach for a source-to-sink link from the chemistry of garnets (2010).
 18. V.K. Shukla, A.K. Rai, A. Diwedi, R. Kumar, A.K. Rai, A quick analysis of various elements (heavy) in sand collected from the topical river (Ganga and Yamuna) using LIBS coupled with multivariate technique. *Natl. Acad. Sci. Lett.* **45**(5), 437–440 (2022)
 19. V.K. Shukla, A.K. Rai, R.K. Verma, A.K. Rai, Investigation of K, Th, U in multiple hoarded granites and their effects in the environment using LIBS coupled with chemometric technique. *Insights Min. Sci. Technol.* **4**(2), 555631 (2023)
 20. V.K. Shukla, A.K. Rai, S. Dubey, and A.K. Rai, Instant identification of sand sample using Laser-induced breakdown spectroscopy, ISSN 2229–3752. <https://sites.google.com/view/laser-and-spectroscopy-society/publication>.
 21. A.K. Rai, J.K. Pati, R. Kumar, Spectro-chemical study of mol-davites from Ries impact structure (Germany) using LIBS. *Opt. Laser Technol.* **114**, 146–157 (2019)
 22. Z. Gazali, S. Thakur, A. Rai, Compositional study of gallbladder stone using photoacoustic spectroscopy. *Opt. Laser Technol.* **111**, 696–700 (2019)
 23. R. Kumar, D.K. Tripathi, A. Devanathan, D.K. Chauhan, A.K. Rai, In-situ monitoring of chromium uptake in different parts of the wheat seedling (*Triticum aestivum*) using laser-induced breakdown spectroscopy. *Spectrosc. Lett.* **47**, 554–563 (2014)
 24. S. Pandhija, A. Rai, In situ multi-elemental monitoring in coral skeleton by CF-LIBS. *Appl. Phys. B* **94**, 545–552 (2009)
 25. W.J. Maniscalco, Optical and electronic properties of rare earth ions in glasses. *Rare Ear. Dop. Fib. Las. Amp.*
 26. L.-B. Mvélé, S. Sasaki, P. Deniard, Y. Tsujimoto, E. Janod, C. Guillot-Deudon, Maria Teresa Caldes, Isabelle Braem, Benoit Corraze, Stéphane Jobic and Laurent Cario, Synthesis of non-centrosymmetric, metastable rare-earth oxysulfides by anionic redox topochemistry. *Chem. Mater.* **35**(18), 7597–7604 (2023)
 27. A. Vishina, O. Eriksson, H.C. Herper, Stable and metastable rare-earth-free permanent magnets from a database of predicted crystal structures. *Acta. Mater.* (2023). <https://doi.org/10.1016/j.actamat.2023.119348>
 28. A. Dwivedi, K. Mishra, S. Rai, Tm³⁺, Yb³⁺ activated ANbO₄ (A= Y, Gd, La) phosphors: a comparative study of optical properties (downshifting and upconversion emission) and laser-induced heating effect. *J. Phys. D Appl. Phys.* **50**, 045602 (2016)
 29. H. Li, W. Sheng, S.A. Haruna, M.M. Hassan, Q. Chen, Recent advances in rare earth ion-doped upconversion nanomaterials: from design to their applications in food safety analysis. *Compr. Rev. Food Sci. Food Saf.* **22**(5), 3732–3764 (2023)
 30. G. Rustad, K. Stenersen, Modeling of laser-pumped Tm and Ho lasers accounting for upconversion and ground-state depletion. *IEEE J. Quantum Electron.* **32**(9), 1645–1656 (1996)
 31. Z. Mahmoud, O. Emad Khalaf, M. Alwan Farhan, Novel photo-synthesis of CeO₂ nanoparticles from its salt with structural and spectral study. *Egypt. J. Chem.* **62**, 141–148 (2019)
 32. V. Rai, L. Tiwari, S. Thakur, D. Rai, Electret microphone for use in photoacoustic spectrometer and photoacoustic spectrum of some rare earth oxide powders. *Pramana* **19**, 579–592 (1982)
 33. M. Negahdary, A. Habibi-Tamijani, A. Asadi, S. Ayati, Synthesis of zirconia nanoparticles and their ameliorative roles as additives concrete structures. *J. Chem.* (2013). <https://doi.org/10.1155/2013/314862>
 34. M. Molli, A. Bhat Kademane, P. Pradhan, V. Sai Muthukumar, Study of nonlinear optical absorption properties of V₂O₅ nanoparticles in the femtosecond excitation regime. *Appl. Phys. A* **122**, 1–4 (2016)
 35. G.H. Brittain, *Profiles of drug substances, excipients and related methodology* (Academic Press, New York, 2016)
 36. P. Dobrowolska, A. Krajewska, M. Gajda-Rączka, B. Bartosewicz, P. Nyga, B.J. Jankiewicz, Application of Turkevich method for gold Nanoparticles synthesis to fabrication of SiO₂@ Au and TiO₂@ au Core-Shell nanostructures. *Materials* **8**, 2849–2862 (2015)
 37. B. Durairaj, T. Xavier, S. Muthu, Fungal generated titanium dioxide nanopartilces for UV Protective and bacterial resistant fabrication. *Int. J. Eng. Sci. Technol.* **6**, 621 (2014)
 38. K. Klačanová, P. Fodran, P. Šimon, P. Rapta, R. Boča, V. Jorík, M. Miglierini, E. Kolek, L. Čaplovič, Formation of Fe (0)-nanoparticles via reduction of Fe (II) compounds by amino acids and their subsequent oxidation to iron oxides. *J. Chem.* (2013). <https://doi.org/10.1155/2013/961629>
 39. M.B. Sreedhara, H.S.S.R. Matte, A. Govindaraj, CNR Rao, Synthesis, characterization, and properties of few-layer MoO₃. *Chem. Asian J.* **8**(10), 2430–2435 (2013)
 40. T.L. Thiem, R.H. Salter, J.A. Gardner, Y.I. Lee, J. Sneddon, Quantitative simultaneous elemental determinations in alloys using laser-induced breakdown spectroscopy (LIBS) in an ultra-high vacuum. *Appl. Phys.* **48**(1), 58–64 (1994)

Publisher's Note Springer Nature remains neutral with regard to jurisdictional claims in published maps and institutional affiliations.

Springer Nature or its licensor (e.g. a society or other partner) holds exclusive rights to this article under a publishing agreement with the author(s) or other rightsholder(s); author self-archiving of the accepted manuscript version of this article is solely governed by the terms of such publishing agreement and applicable law.